JOINT EUROPEAN TORUS JET

JET–P(88)47

A. Cheetham
and JET Team

Pellet Fuelling of Tokamaks

Pellet Fuelling of Tokamaks

A. Cheetham
and JET Team*

JET-Joint Undertaking, Culham Science Centre, OX14 3DB, Abingdon, UK

** See annex of P. Lallia et al, "Plasma Heating in JET",*
(13th EPS Conference on Controlled Fusion and Plasma Physics, Schliersee, Germany (1986)).

Preprint of Paper to be submitted for publication in
Invited Article for Europhysics News

Electron Heating During ICRH in JET

L.G. Eriksson* and T. Hellsten

JET Joint Undertaking, Abingdon, Oxon. OX14 3EA, UK

*Chalmers University of Technology, S-41296 Gothenburg, Sweden.

Abstract

Electron heating during ICRH in the JET tokamak is studied. Electron heating profiles are obtained by measuring the increase in electron temperture after sawtooth crashes. By studying the increase in electron heating during power ramp-up it is possible to distinguish direct electron heating from indirect electron heating via minority ions. For direct heating, power deposition profiles are obtained and compared with code calculations. For indirect electron heating the time dependence is consistent with classical slowing down of high energy ions on electrons through Coulomb collisions.

1. INTRODUCTION

Collisionless absorption of waves in the ion cyclotron range of frequencies occurs either by ion cyclotron absorption or by electron Landau (ELD) and transit time damping (TTMP). In cases where the antennae excite the magnetosonic wave, absorption occurs either directly by these processes or indirectly via mode conversion. Linear as well as non-linear mode conversion of the magnetosonic wave into kinetic waves can take place. Both ion cyclotron absorption, by a resonating minority species, as well as direct electron absorption results in electron heating. However, the electron heating takes place on two different time scales. Electron heating

via energy transfer from minority ions occurs after a high energy tail of the resonating ions has been formed. We refer to this electron heating as indirect electron heating. The indirect electron heating should saturate on the timescale of fast ions collisional slowing down on electrons which is typically 0.2-1s in present JET experiments. Electron heating through electron Landau damping, ELD, and transit time damping, TTMP, which we refer to as direct electron heating, should take place on the timescale given by electron-electron collisions which is typically of the order of ms. This difference in the timescales can be used to separate the two damping mechanisms by studying the variation of the electron temperature during ion cyclotron heating. In the present paper, this is done by measuring the time derivatives of the electron temperature after so-called sawtooth crashes during ramp-up and ramp-down of the coupled RF-power. Due to the short timescale for thermalisation of the electrons the direct electron heating is expected to increase linearly with increasing RF-power. On the other hand, in the case of indirect electron heating the relationship becomes much more complicated, especially when the RF-ramp time is comparable with the slowing down time. A simplified model equation is presented in Section 2.1. Good, qualitative, agreement has been obtained between numerical solutions of this model equation and experimental values. The results indicate that the electrons are heated via Coulomb collisions with the minority ions, and that the fast ions are at least partially confined in the central region during a sawtooth crash.

We have analyzed a number of different heating scenarios in JET such as minority heating of ^{3}He in a ^{4}He-plasma, ^{3}He in a D-plasma and H in a D-plasma. The frequency and magnetic field were chosen such that the ion cyclotron resonances of the resonating ion species passes close to the magnetic axis. The electron heating by ICRH is different in the various heating scenarios, for some of them the electron heating occurs essentially

via minority ion heating, in others the electron heating occurs via direct electron heating and for some scenarios both processes take place.

2. ANALYSIS OF THE ELECTRON HEATING PROFILE FROM THE SAWTOOTH SLOPE

In a tokamak plasma the electron temperature usually oscillates with respect to time due to so-called sawtooth activity [1]. As an example of such oscillations we show in Fig. 1 the time variation of the electron temperature at a central position in the plasma during ICRH. The electron temperature is obtained by measuring the intensity of the electron cyclotron emission from the plasma for various frequencies; the frequency determining the strength of the magnetic field from which the emission originates. With the use of equilibrium calculations, the spatial emission can be obtained. The twelve-channel grating polychromator [2] measures the temporal evolution of the electron temperature at twelve positions along the major radius of the plasma. An advantage with using the polychromator for measuring the electron temperature is that the position of the ion cyclotron resonance can be directly related to the channels by the frequency of the ECE-signal. The variation of the electron temperature profile in the mid plane is shown in Fig. 2 as obtained with the Michelson interferometer [3].

To determine the local energy increase we make use of the 2mm microwave interferometer [4] measuring the line averaged density. When evaluating the energy increase in the electrons after a sawtooth crash, we assume the density to be constant during the initial rise. The energy increase of the electrons versus coupled RF-power is shown in Fig. 3 for two heating scenarios and versus time of the consecutive sawteeth in Fig. 4. For some heating scenarios the local electron energy increase after a sawtooth crash is a linear function of the coupled power (e.g. discharge #13683). For

other scenarios the energy increase is a non-linear function of the coupled power (e.g. discharge #13734).

2.1 Analysis of Electron Heating

After a sawtooth crash, the electron temperature profile becomes almost flat in the centre, see Fig. 2, and hence the energy conduction becomes small. The electron heat conduction equation can therefore be approximated by

$$\frac{d}{dt}\left(\frac{3}{2} nkT_e\right) = \eta j^2 - \frac{1}{\tau_{ie}} nk(T_e - T_i) - P_{rad} + P_{RFD} + P_{RFI} \qquad (1)$$

where η is the resistivity, j is the current density, τ_{ie} is the energy transfer time between ions and electrons, P_{rad} is the radiation losses, P_{RFD} is the direct RF-power density going to the electrons and P_{RFI} is the power density due to power transfer from the heated minority ions.

The radiation losses in the centre are dominated by line radiation from Ni and are much smaller than the local heating [6]. Power transfer due to equipartion between electrons and ions, the second term on the r.h.s. in Eq. (1), can in some cases be appreciable. However, the main contributions to the r.h.s. of Eq. (1) comes from the ohmic term and the direct/indirect RF-heating terms. Thus, if direct electron heating dominates over indirect electron heating, and the ohmic heating stays roughly constant, one would expect to see a linear relation between the coupled power and the electron heating after sawtooth crashes during a ramp up or a ramp down of the coupled power. The power density due to direct electron heating by ICRH can then be obtained from the slope of the curve (for discharge #13683) in

Fig. 3. On the other hand, if indirect heating dominates, the relation can be expected to be nonlinear.

In order to get a qualitative understanding of the indirect heating, we study the following simplified Fokker-Planck equation

$$\frac{\partial f}{\partial t} = Q_{RF}(f) + \frac{1}{v^2}\frac{\partial}{\partial v}\left[\frac{v^3 f}{t_s}\right] - \frac{f}{t_l} \tag{2}$$

where f is the distribution function, Q_{RF} is the RF-operator [7] t_s is the slowing down time for ion-electron collisions and t_l is an equivalent loss time. The approximation of the collisions with only the electron slowing down term is justified if the RF-power density per minority ion is high enough, this is often the case in the centre even for moderate RF-powers.

Multiplying Eq. (2) with $\frac{1}{2}mv^2$ and integrating yields

$$\frac{dW_f}{dt} = p_{RF}(t) - \frac{2}{t_s} W_f - \frac{1}{t_l} W_f \tag{3}$$

where W_f is the energy content per unit volume of the minority ions, and $p_{RF}(t)$ is the RF-power density.

The solution to Eq. (3) can be written as

$$W_f = \exp\left[-\int_o^t \left(\frac{2}{t_s} + \frac{1}{t_l}\right)dt'\right]\left\{\int_o^t p_{RF}(t) \exp\left[\int_o^{t'} \left(\frac{2}{t_s} + \frac{1}{t_l}\right)dt''\right]dt' + W_f(t=0)\right\} \tag{4}$$

The indirect electron heating is then obtained as

$$p_e = \frac{2}{t_s} W_f \tag{5}$$

If one neglects losses and approximates t_s by a constant, one obtains for a linear ramp up of the RF-power ($p_{RF}(t) = \frac{t}{t_R} p_o$)

$$p_e/p_o = \frac{t}{t_R} - \frac{t_s}{2t_R} (1-e^{-\frac{2t}{t_s}}) \tag{6}$$

or

$$p_e/p_o = x - \frac{t_s}{2t_R} (1-e^{-\frac{2t_R}{t_s} x}) \tag{7}$$

where $x = p_{RF}(t)/p_o$. For small x we obtain

$$p_e/p_o = \frac{t_R}{t_s} x^2 \tag{8}$$

The sequence for a ramp up during $0 < t < t_R$, a constant power phase during $t_R < t < 2t_R$ and a ramp down during $2t < t < 3t_R$ is shown in Fig. 5. Note the hysteresis effect in electron heating. The value of t_R/t_s is 3.3 in Fig. 5.

The situation becomes much more complicated for a real case with a sawtoothing electron temperature. In addition, it is not clear what happens to the fast ions during a sawtooth crash. However, it is possible to obtain some insight into the indirect heating by taking the experimental data for the electron temperature and the coupled power and integrate Eq. (4) numerically. Different models for the loss term can then be used to study the effects of losses of fast particles during a sawtooth crash. The dashed line in Fig. 3 has been obtained by this method, with the losses assumed to be small. The calculated curve is normalized to the measured one at the point where P_{RF} = 11MW. As can be seen, the qualitative behaviour is

similar for the calculated points and the measured ones.

3. ANALYSIS OF EXPERIMENT

3.1 A Density Scan of ^{3}He Minority in ^{4}He Plasmas

A series of ICRH experiments were performed in ^{4}He-plasmas with ^{3}He as the minority species, discharges #13675-13698. The RF-frequency was equal to 33.9 MHz chosen such that the cyclotron resonance of ^{3}He passed close to the magnetic axis. Toroidal dipole phasing of the antennae was used, which peaks the spectrum around toroidal mode numbers $n \approx 30$. The axial electron density was about $n_e(0) \approx 4\text{-}4.5 \times 10^{13} cm^{-3}$, $B_o \approx 3.4$ T, $T_e \approx 5\text{-}10$ keV, $T_i \approx 4\text{-}8$ keV and $Z_{eff} \approx 4\text{-}4.5$. Furthermore, the filling pressure of the minority ions, ^{3}He, varied between 5-120 mbar.

The discharges #13683, #13684, #13687 and #13692 all showed a linear relation between the electron heating, p_e, and the coupled power, P_{RF}, indicating that direct electron heating dominated. Their corresponding direct RF-power deposition profiles are shown in Fig. 6. The minority concentration can be estimated, from the density increase when ^{3}He was injected. For the 30 mbar discharge #13684, it was estimated to $n_{^3He}/n_e = 5\%$. It is interesting to note that for the lower filling pressures (15-30 mbar) the deposition profiles are broad and almost identical whereas the 120 mbar discharge gave a much more peaked profile.

Due to the high Z_{eff} in these discharges the ratio $n_{^3He}/n_{^4He}$ becomes large and the ion cyclotron absorption weak (typically $n_{^3He}/n_{^4He} > 15\%$). Since toroidal dipole phasing of the antennae was used the most likely absorption mechanism is direct absorption of the magnetosonic wave by ELD and TTMP. Possible explanations to the peaked profile for the 120 mbar

discharge are either mode conversion or a weaker cyclotron absorption which results in more TTMP and ELD.

We have compared the measured power deposition profiles for direct electron heating with profiles calculated with the LION code [9]. A modified verrsion of the LION code, which takes into account ELD and TTMP, has been used. Two calculated power deposition profiles due to TTMP and ELD are shown in Fig. 6, one with $n_{^3He}/n_e = 0.025$ and one with $n_{^3He}/n_e = 0.05$. The power deposition has been obtained by approximating the coupling spectrum with six toroidal modes. There is a rough agreement between the calculated and measured deposition profiles. In particular, both show broad profiles and the profile becomes more peaked at higher minority concentration.

Figure 7 shows the electron heating, p_e, versus the coupled power, P_{RF}, for discharges #13684, #13688 and #13689. As can be seen in this figure it is only the discharge with the lowest filling pressure (5 mbar) that gives a nonlinear relation between p_e and P_{RF} consistent with indirect electron heating. Discharge #13689, with filling pressure 60 mbar, shows a nonlinear relation between p_e and P_{RF} which is different from what one would expect from indirect heating. We interpret the heating of this discharge as follows: the fraction of the coupled power going to mode conversion decreases as the ion temperature increases. As mentioned before, discharge #13684, with filling pressure 30 mbar, give a linear relation between p_e and P_{RF} indicating that direct electron heating dominated.

Further information can be obtained by studying the energy content of the minority ions. For indirect electron heating the energy content of the minority ions should be large whereas it is expected to be small for direct electron heating. The energy content in the perpendicular minority ion tail, W_f, can be obtained by taking the difference between the change in

energy, $\delta W_{DIA} = \frac{3}{2} W_{\perp}$, based on measurements of the diamagnetic effect and the change in energy, $\delta W_{MHD} = \frac{3}{4} W_{\perp} + \frac{3}{2} W_{||}$, based on MHD equilibrium calculations, viz.

$$W_f = \frac{4}{3} (\delta W_{DIA} - \delta W_{MHD}).$$

Figure 8 shows the estimated fast ion energy contents for discharge #13688 and #13692, as can be seen the fast ion energy content increases significantly for discharge #13688 whereas it remains low for discharge #13692, which is in agreement with the analysis above.

It is interesting to note that both discharges #13688 and #13692 gave rise to sawtooth free periods, whereas the discharges in the 15-30 mbar range did not. Thus, it appears to be possible to create sawtooth free periods with both dominating indirect electron heating as well as with dominating direct electron heating. Furthermore, the fact that the 15-30 mbar discharges did not give rise to sawtooth-free periods might be connected to their much broader deposition profiles.

3.2 Direct Electron Heating with ^{3}He Minority in D Plasmas

In this section we analyse two discharges, one with toroidal dipole phasing of the antenna, #13701, and one with toroidal monopole phasing, #14609.

The parameters for discharge #13701 was as follows: $n_e(0) \approx 4.2 \times 10^{19}$ m^{-3}, $T_e \approx 7.5$ keV, $T_i \approx 4$ keV, $B_T \approx 3.48$T, $f \approx 33.9$ MHz, $Z_{eff} = 4.5$. The discharge showed a linear dependence between p_e and P_{RF}, indicating direct electron heating dominates. Again, this is not very surprising since Z_{eff} was high and therefore the ratio n_{3He}/n_D is also high. Figure 9 shows the

corresponding direct electron heating deposition profile. The deposition profile is very broad and almost identical to those of 15-30 mbar ^{3}He in ^{4}He plasmas. Furthermore, since dipole antenna was used, the absorption is most likely due to TTMP and ELD.

Toroidal monopole phasing, which peaks the spectrum around toroidal mode number n = 0, of the antenna was used in the second discharge, #14609, with the following parameters: $n_e(0) \approx 3.7 \times 10^{19} m^{-3}$, $T_e(0) \approx 6$ keV, $T_i(0) \approx 4$ keV, $B_T \approx 3.47$T, f = 32.1 MHz, $Z_{eff} = 1.9$. The electron heating, p_e, versus the coupled power, P_{RF}, is shown in Fig. 10. There are essentially two linear regions; one for low RF-powers and one for high RF-powers. We interpret this as mode conversion which decreases as the ion temperature increases. By taking the slope of T_e for low RF-powers, we should be able to measure the direct electron heating profile due to mode conversion. This profile is shown in Fig. 10. The deposition profile is extremely peaked, which is consistent with mode conversion.

3.3 Indirect Heating of H Minority in D-Plasmas

Here we analyse two discharges #7218 and #7220 which were dominated by indirect heating. The hydrogen concentration n_H/n_D was approximately 3%. A prominent feature of discharge #7220 is the hysteresis effect which is obtained when the coupled power is ramped up and down, Fig. 11. A numerical solution of Eq. (5) using the experimental data for the electron temperature, RF-power etc. is also shown in Fig. 11. The theoretical curve has been normalized at $P_{RF} = 4.38$ MW. The qualitative features, i.e. the shape of the curves, are in good agreement. It is interesting to note that the shape of the theoretical curve is almost unchanged if one assumes no losses or losses of about 50% of the fast ion energy content during a sawtooth

crash. It is therefore difficult to determine the fast ion losses from this analysis.

In discharge #7218 the RF-power was applied without a ramp. Figure 12 shows the electron heating profile for this discharge. The electron heating can here be seen to saturate on a time-scale comparable to that of fast ions slowing down on the electrons. For this discharge the slowing down time was 0.3s. Furthermore, the electron heating continues after the RF-power is switched off.

These two discharges demonstrate that the electron-heating occurs due to slowing down of fast ions on electrons. Furthermore, the results are consistent with classical slowing down.

4. DISCUSSIONS

Power deposition due to direct electron absorption in the central parts of the plasma can be obtained by studying the electron energy increase as the coupled RF-power is ramped up and down. For heating scenarios for which direct electron heating dominates, we have found that the electron heating usually is a linear function of the coupled RF-power, both when the power is ramped up as well as down. For such cases the increase in the electron heating can be separated into direct electron absorption of the RF-waves and the sum of ohmic heating, losses of energy due to radiation and energy transfer to ions. Rather accurate power deposition profiles can be obtained since the local power deposition is determined by several measurements.

For the case of high minority concentrations, dominating direct electron heating has been observed. For intermediate minority concentrations with the dipole phasing of the antennae a broad power deposition profile is obtained for the direct electron heating. Due to the large toroidal mode number no mode conversion should take place. TTMP and ELD are then the most likely absorption mechanisms in these cases. For the highest

concentration of minority ions the deposition profile becomes more peaked. This could be explained by mode conversion but also by a weaker cyclotron absorption, which leads to a larger fraction of the power being absorbed by ELD and TTMP. Comparison between the power deposition profile due to TTMP and ELD of the magnetosonic wave as calculated with a modified version of the LION-code and the measured profiles, shows reasonable agreement. However, for comparison with code calculations the estimate of the minority concentration becomes critical. The uncertainty in the comparison is therefore substantial. In the case of monopole antenna, the deposition profile, deduced from the electron heating at the beginning of the RF-power ramp, is very peaked. It is possible that mode conversion might have played an important role here, which would explain the peaked profile.

In the case when the electron heating is dominated by indirect heating the electron heating increases on a time scale of high energy ions slowing down on electrons. Theoretical calculations of the electron heating are in good qualitative agreement with the measured values. Furthermore, the results indicate that indirect electron heating dominates for low minority concentrations.

The obtained indirect electron heating profile will not necessarily be related to the RF-power absorption profile. Instead it is related to the spatial distribution of high energy ions after a sawtooth crash. Due to the reduction of the electron temperature after the swawtooth crash the energy transfer from these ions to the electrons becomes faster. The good agreement with the calculated and the measured values are consistent with a non negligible part of the ions being confined near the centre after sawtooth crashes and that the slowing down of the high energy ions occurs via Coulomb collisions. The presence of indirect heating is also confirmed by the fact that the electron heating continues after the RF-power is switched off.

Periods of sawtooth free activity which has been observed on JET occurs both when direct electron absorption dominates or when indirect electron heating dominates. In particular, for the series of discharges with minority heating of ^{3}He in ^{4}He-plasma, sawtooth free periods were obtained for both the high and low minority concentrations, but not for the intermediate concentrations.

ACKNOWLEDGEMENTS

The authors wish to thank the ECE-group for providing the measurements of the electron temperature, the RF-group and operation teams for providing the discharges which have been analysed. They are also very grateful to Drs. D.J. Campbell and D.F. Düchs for valuable discussions concerning the manuscript.

References

[1] Von Goeler, S., Studiek W. and Sauthoff, N. Phys. Rev. Letts. 33 (1974) 1201.

[2] Tubbing, B.J.D., Barbran, E. Campbell, D.J., Hugenholtz, C.A.J. et al., in Contr. Fusion and Plasma Physics, Proc. 12th European Conference, Budapest 1985, 9F-I (1985) 215.

[3] Costley, A.E., Baker, E.A.M., Brusati, M., Bartlett, D.V. et al., in Controlled Fusion and Plasma Physics, Proc. 12th European Conf., Budapest 1985, 9F-I (1985) 227.

[4] Fessey, J.A., Gowers, G.W., Hugenholtz, C.A.J. and Slavin, K. J. Phys. E: Sci. Instrum. 20 (1987) 169.

[5] Bartiromo, R., Bracco, G., Brusati, M., Grosso, G., Mantovani, S., Tillia, B. and Zanza, V. Rev. Sci. Instr. 58 (1987) 788.

[6] Engelhardt, W.W. et al., Plasma Physics and Controlled Fusion 28 (1986) 1401.

[7] Stix, T. Nucl. Fusion 15 (1975) 737.

[8] Villard, L., Appert, K., Gruber, R. and Vaclavik, J. Comput. Phys. Reports 4 (1986) 95.

[9] Llobet, X., Hellsten, T. and Villard, L. Proc. Joint Varenna-Lausanne International Workshop on "Theory of Fusion Plasma", Chexbres, October 1988.

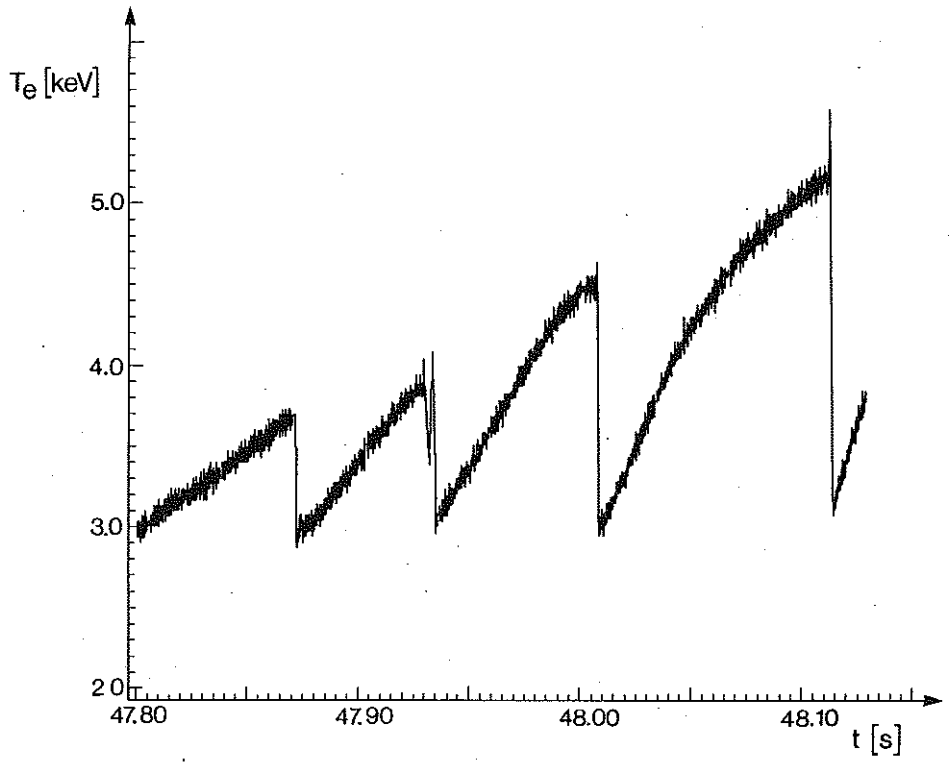

Fig. 1 The variation of the central electron temperature during RF-heating for discharge # 11152.

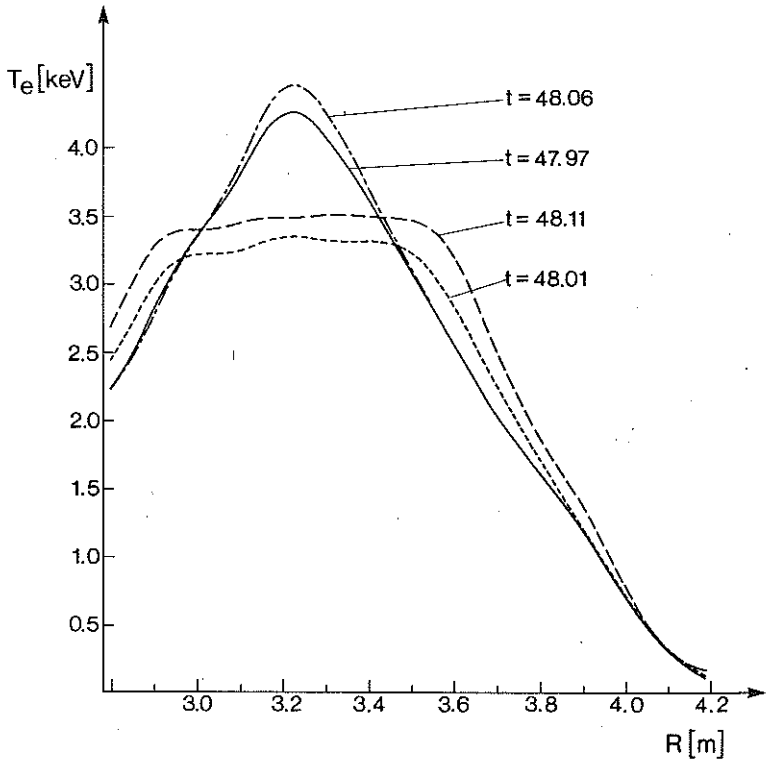

Fig. 2 Temperature profiles during sawtoothing for discharge # 11152. (——) t=47.97 s, (. . . .) t=48.01 s, (–.–.–) t=48.06 s, (– – –) t=48.11 s.

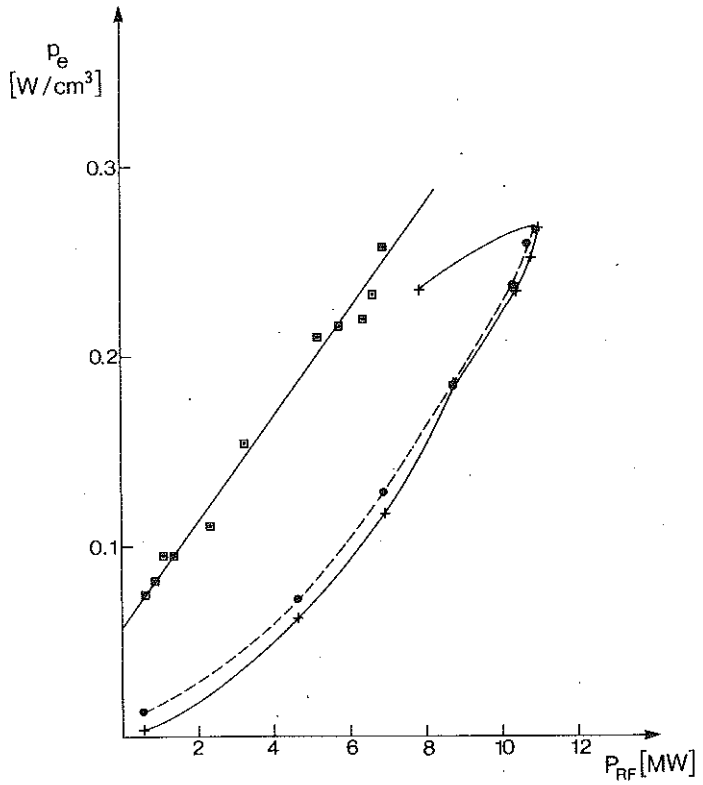

Fig. 3 The increase of the electron energy after a sawtooth crash, p_e, versus coupled RF-power, P_{RF}, for discharges # 13683 (⊡) and # 13734 (+). The (●) represents calculated values for Eqs. (4,5) for # 13734.

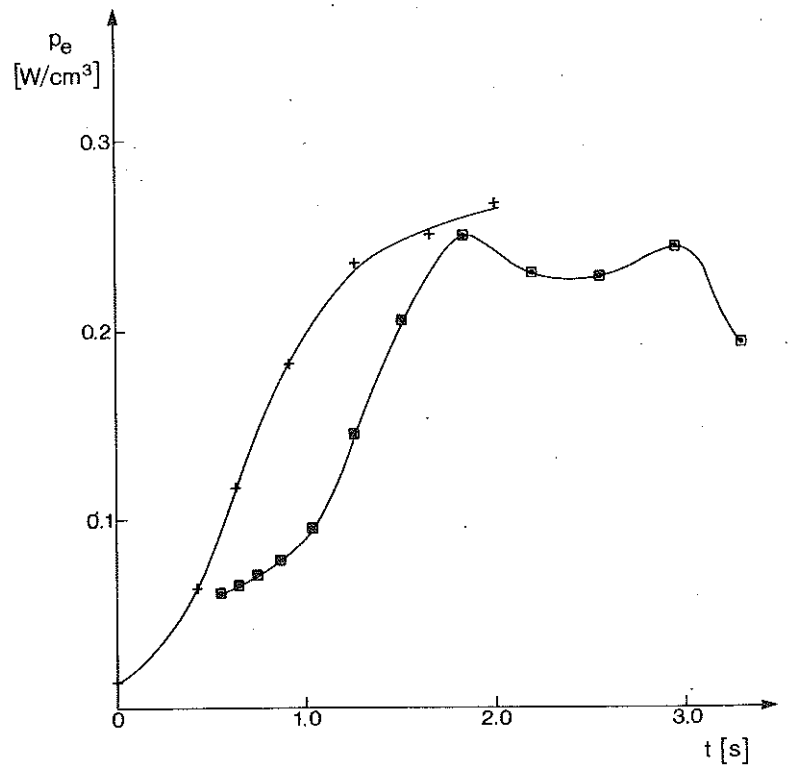

Fig. 4 The increase of the electron energy after a sawtooth crash, p_e, versus time, t, for the discharges # 13683 (⊡) and # 13734 (+).

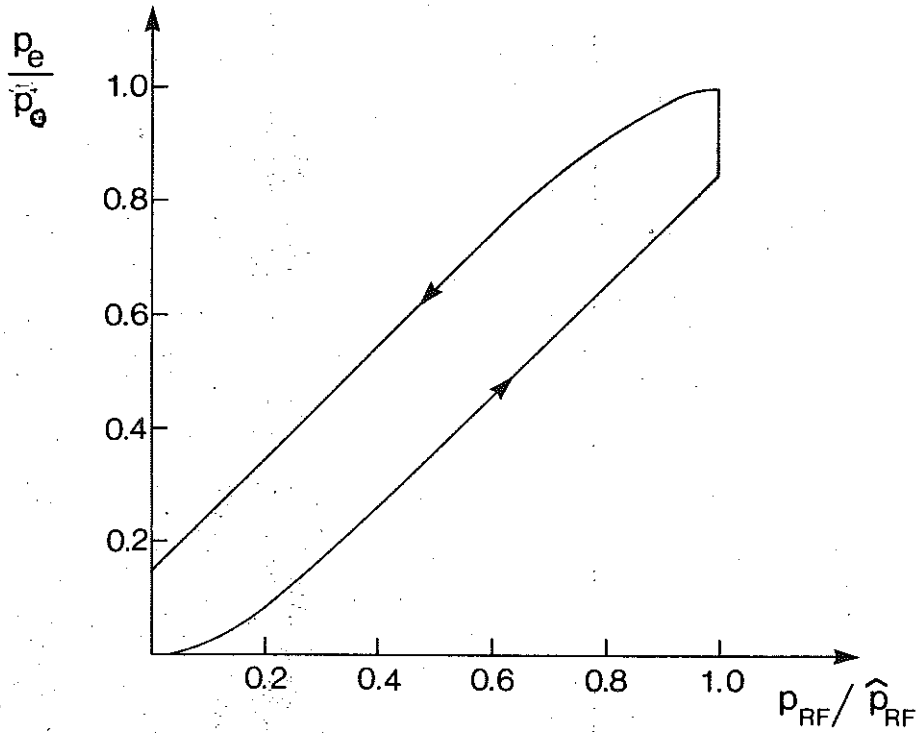

Fig. 5 Electron heating versus local RF-power absorption during a linear ramp up, constant power phase and a linear ramp down for $t_s = 0.3$ s and $t_R = 1$ s. The arrow shows the time sequence.

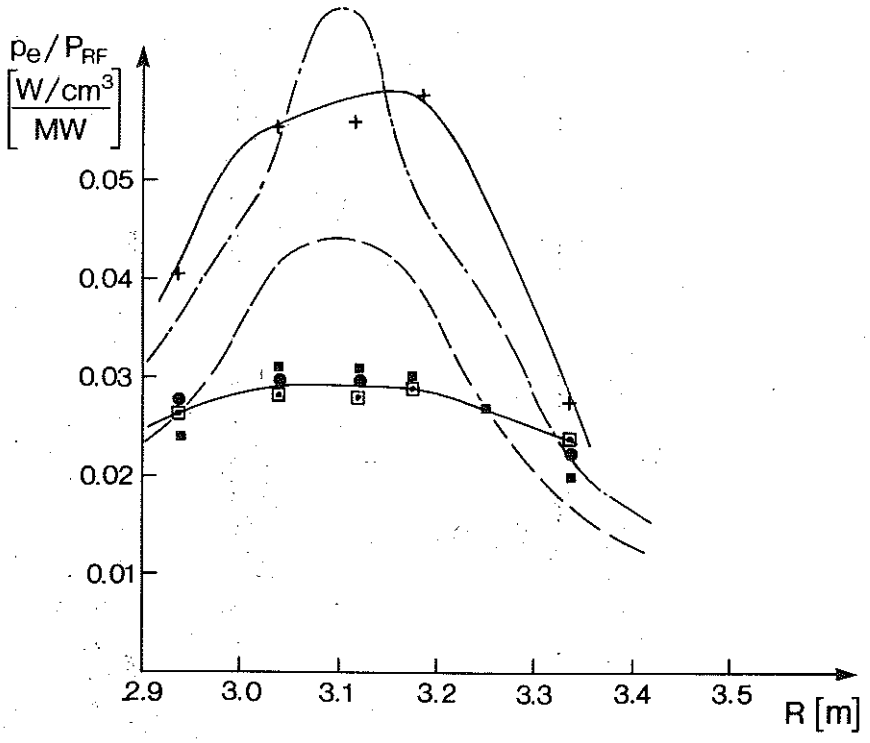

Fig. 6 Electron heating profiles for discharges # 13683 (⊡), # 13684 (●), # 13687 (▪), # 13692 (+). Calculated profiles for $n_{^3He}/n_e = 0.025$ (– – –), $n_{^3He}/n_e = 0.05$ (–.–.–).

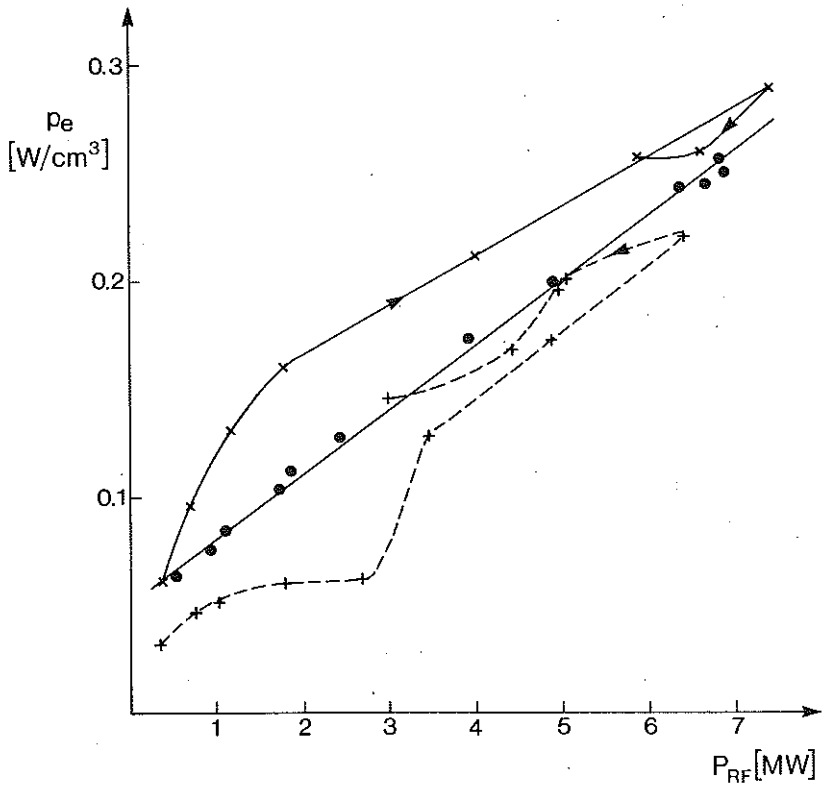

Fig. 7 The increase of the electron energy after a sawtooth crash, p_e, versus coupled RF-power for discharges # 13684 (•) with filling pressure 30 mbar, # 13688 (+) with filling pressure 5 mbar, # 13689 (x) with filling pressure 60 mbar. The arrows show the time sequence.

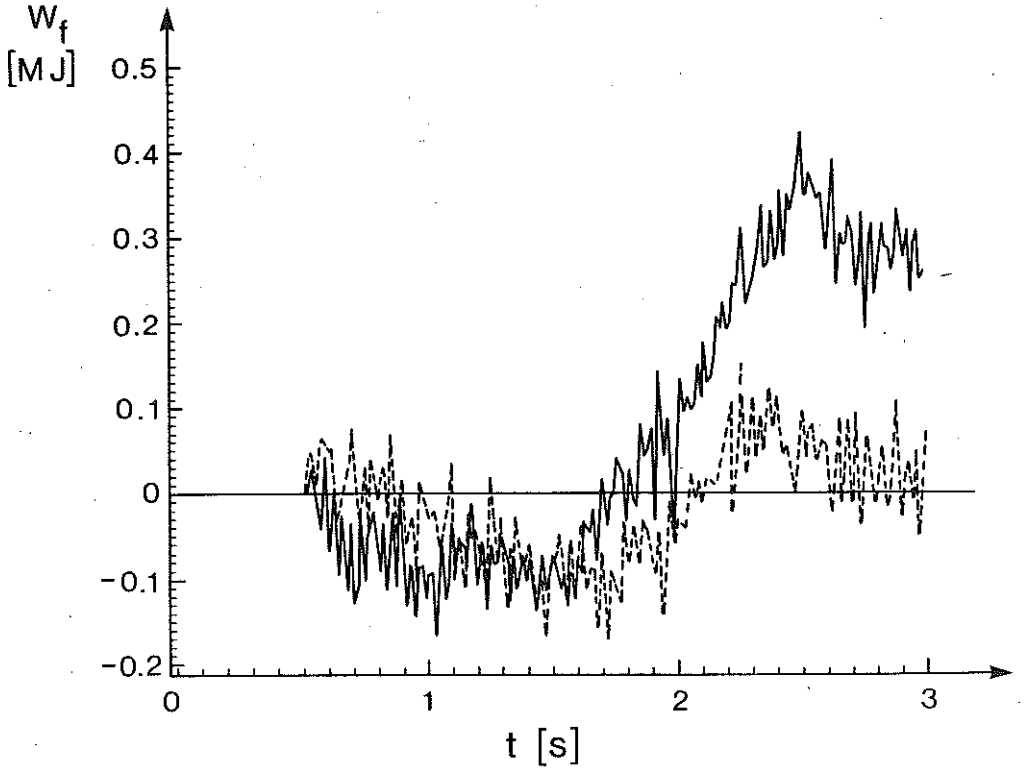

Fig. 8 Fast ion energy content for discharges # 13688 (5 mbar) full line and # 13692 (120 mbar) dashed line. The RF-power is ramped during $t=2$ s to $t=3$ s and then reaches a flat top.

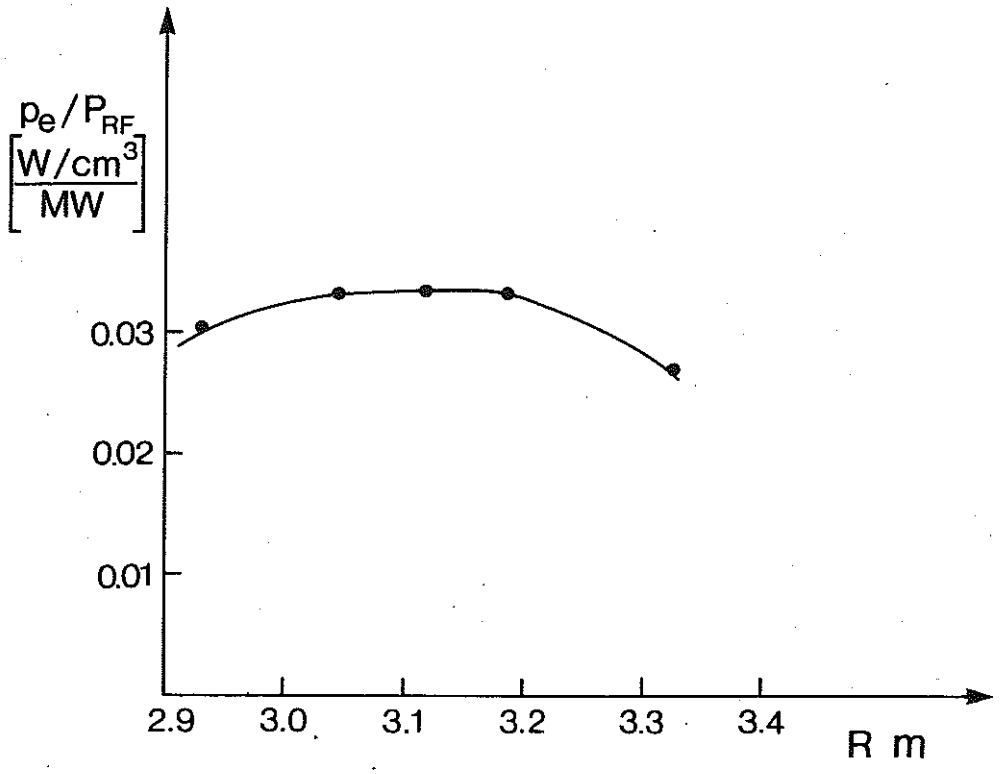

Fig. 9 Direct electron heating profile for discharge # 13701.

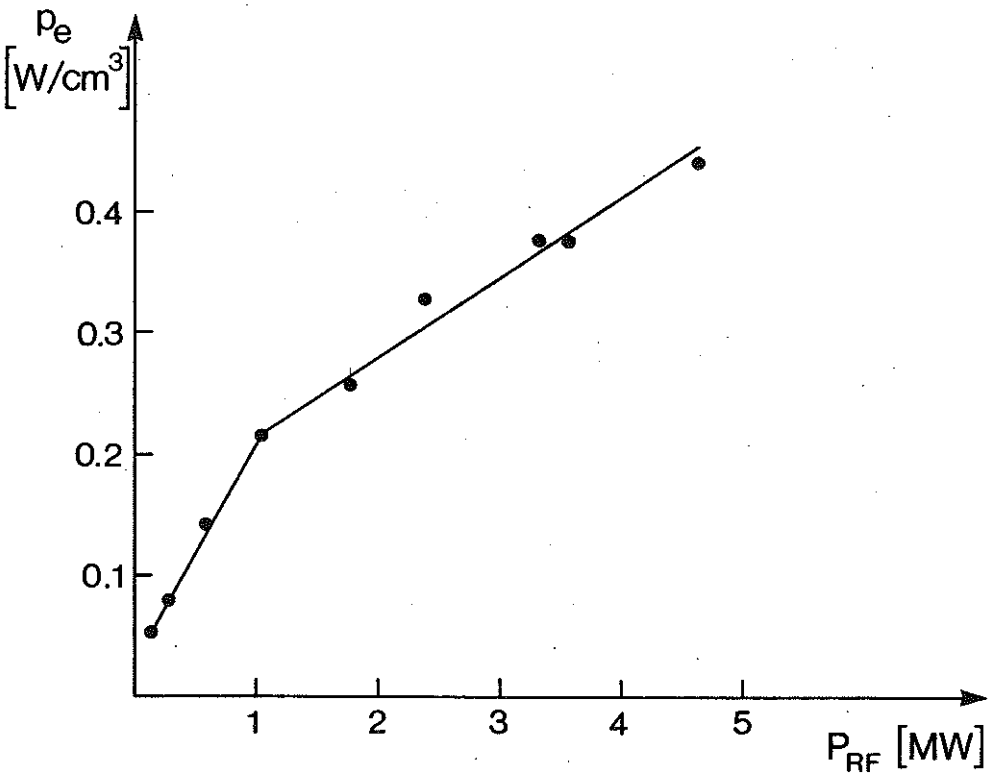

Fig. 10 The increase of electron energy after a sawtooth crash, p_e, versus coupled power, P_{RF}, for discharge # 14609.

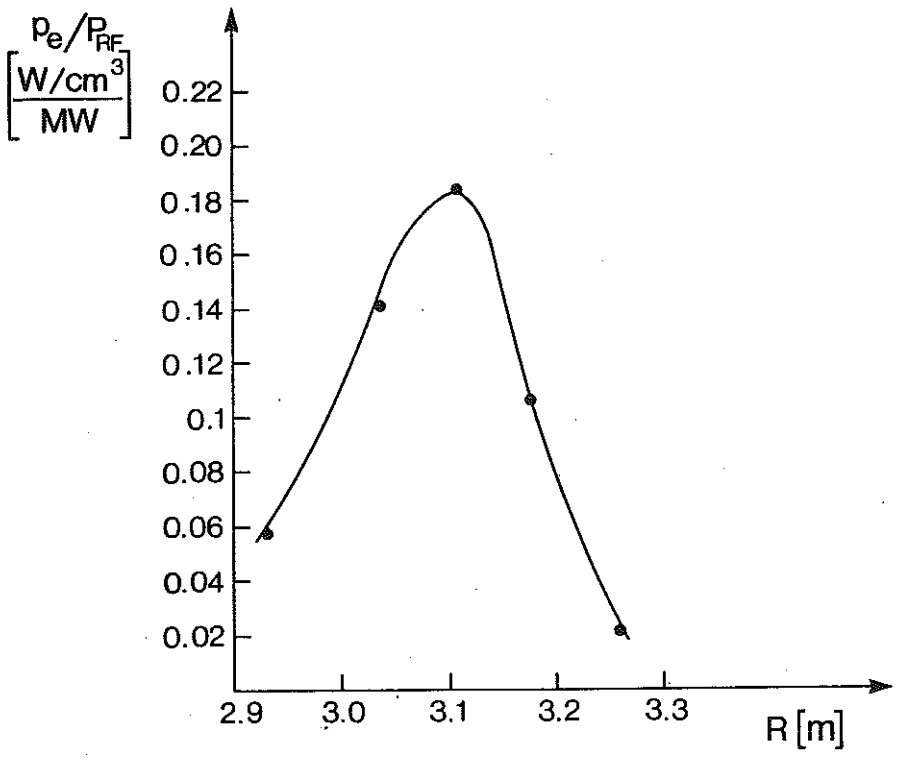

Fig. 11 Direct electron heating profile for discharge # 14609.

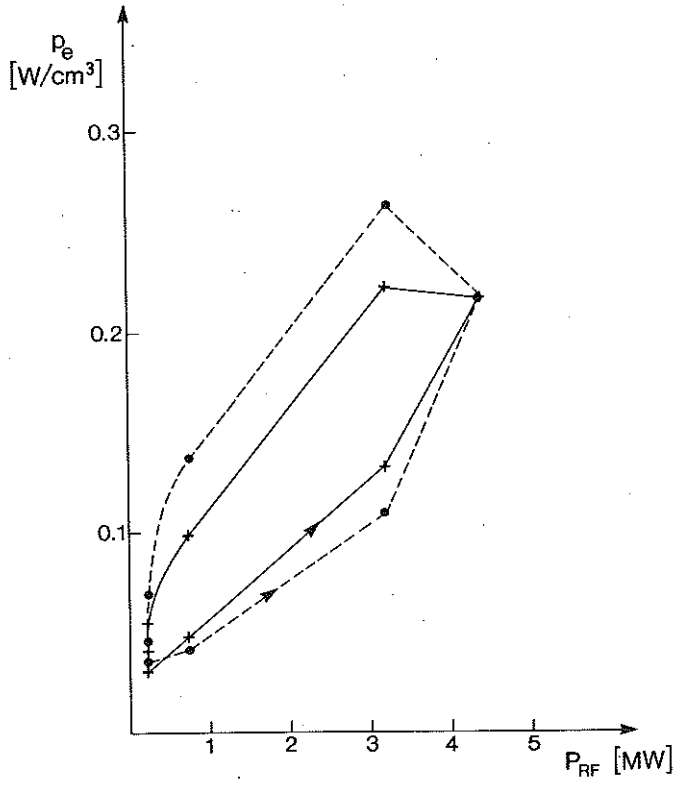

Fig. 12 The increase of electron energy after a sawtooth crash, p_e, versus coupled power for discharge # 7220. The arrow shows the time sequence. The measured values are indicated by (+) and the calculated from Eqs. (4,5) by (●).

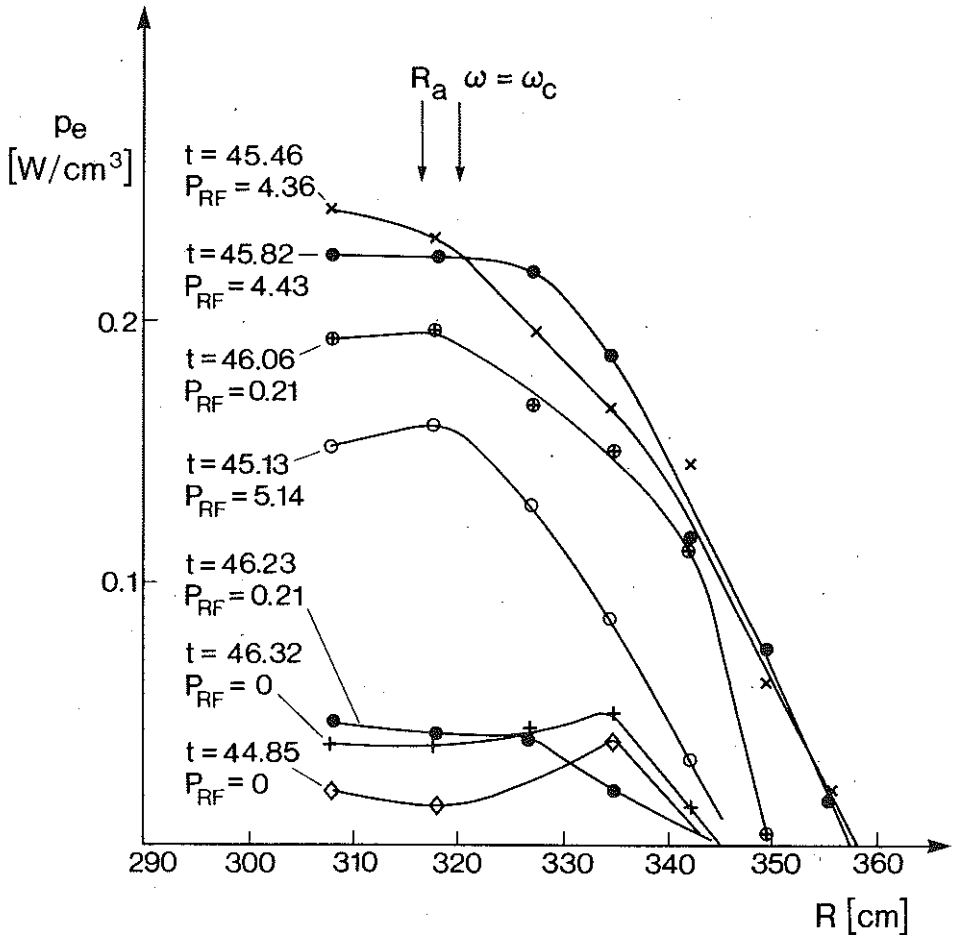

Fig. 13 Electron heating profile for discharge #7218 at different times. The position of the cyclotron resonance is shown with an arrow.